Climate Dynamics (2005) 25: 517–535
DOI 10.1007/s00382-005-0056-x

Alessandra Giannini · R. Saravanan · Ping Chang

Dynamics of the boreal summer African monsoon in the NSIPP1 atmospheric model

Received: 9 February 2005 / Accepted: 15 June 2005 / Published online: 13 August 2005

Abstract A nine-member ensemble of simulations with a state-of-the-art atmospheric model forced only by the observed record of sea surface temperature (SST) over 1930–2000 is shown to capture the dominant patterns of variability of boreal summer African rainfall. One pattern represents variability along the Gulf of Guinea, between the equator and 10°N. It connects rainfall over Africa to the Atlantic marine Intertropical Convergence Zone, is controlled by local, i.e., eastern equatorial Atlantic, SSTs, and is interannual in time scale. The other represents variability in the semi-arid Sahel, between 10°N and 20°N. It is a continental pattern, capturing the essence of the African summer monsoon, while at the same time displaying high sensitivity to SSTs in the global tropics. A land–atmosphere feedback associated with this pattern translates precipitation anomalies into coherent surface temperature and evaporation anomalies, as highlighted by a simulation where soil moisture is held fixed to climatology. As a consequence of such feedback, it is shown that the recent positive trend in surface temperature is consistent with the ocean-forced negative trend in precipitation, without the need to invoke the direct effect of the observed increase in anthropogenic greenhouse gases. We advance plausible mechanisms by which the balance between land–ocean temperature contrast and moisture availability that defines the monsoon could have been altered in recent decades, resulting in persistent drought. This discussion also serves to illustrate ways in which the monsoon may be perturbed, or may already have been perturbed, by anthropogenic climate change.

A. Giannini (✉)
International Research Institute for climate prediction,
The Earth Institute at Columbia University,
P. O. Box 1000, Palisades, NY 10964-8000, USA
E-mail: alesall@iri.columbia.edu
Tel.: +1-845-6804473
Fax: +1-845-6804864

R. Saravanan
National Center for Atmospheric Research, Boulder, CO, USA

P. Chang
Department of Oceanography, Texas AM University, College Station, TX, USA

1 Introduction

One of the outstanding problems of recent times in tropical climate dynamics has been to understand the cause(s) of the recurrent droughts that plagued the African Sahel during the 1970s and 1980s. The Sahel, the transition region between the humid tropical rainforest to the south and the Sahara desert to the north, is characterized in the climatological mean by a steep meridional gradient in total annual rainfall—a one order of magnitude decrease from 1,000 mm accumulated at its equatorward limit to 100 mm accumulated at its poleward limit—and by variability that increases as the mean decreases, with the standard deviation rising from 10–20% of the mean at the southern edge to 50% at the northern edge (Nicholson 1980).

The high variability, hence the potential for high vulnerability to climate of this semi-arid region is a consequence of its geographical location, at the northern edge of the area influenced by the African monsoon in its annual meridional migration following the sun. The rainy season at the poleward edge of the Sahel is on average limited to the three-month period immediately following the northern summer solstice, when the monsoon reaches its most northern location. Failure of the monsoonal circulation to migrate north during this short window of time can have serious consequences for an environment that is already dry for the better part of a year.

Total annual rainfall in the Sahel was above average during the 1950s and early 1960s, then steadily decreased from the late 1960s through the 1970s and 1980s. The decline was punctuated by major widespread episodes of drought and famine, e.g., in 1972–1973 and 1982–1984 (Nicholson 1979, 1980, 1993; also see, e.g., issues of the National Geographic Magazine in April 1974, August

1975, and August 1987). The persistence of anomalously dry year-to-year conditions in the late 1960s and early 1970s (Glantz and Katz 1985) prompted scientists to hypothesize that something had gone awry in the environment of tropical North Africa, and that change in the form of human-induced desertification, e.g., loss of vegetative cover caused by the farming and overgrazing of marginal lands to satisfy the needs of an ever-increasing population, had set in (Otterman 1974; Charney 1975).

The recent success of atmospheric models, of simpler (Zeng et al. 1999) or more complex design (Bader and Latif 2003; Giannini et al. 2003) in replicating the spatio-temporal characteristics of observed Sahel rainfall variability when forced only with the observed history of sea surface temperature (SST) scores a decisive point in favor of an alternative hypothesis, that climate in the Sahel is sensitive to global conditions, more precisely to global tropical SST anomalies, as hypothesized by earlier observational and modeling studies (Lamb 1978a, 1978b; Folland et al. 1986; Palmer 1986; Rowell et al. 1995; Janicot et al. 1996; Fontaine et al. 1998). Such success has revitalized the interest in the potential for application of seasonal climate prediction in the Sahel to early warning systems in food security and health (Thomson et al. 2000; Traoré 2003; Palmer et al. 2004).

The purpose of this study is to document in detail statistical and dynamical aspects of the simulation of the boreal summer African monsoon obtained with NSIPP1—version 1 of the atmospheric model developed at the National Aeronautics and Space Administration (NASA)'s Goddard Space Flight Center in the framework of the Seasonal to Interannual Prediction Project. A nine-member ensemble of integrations forced only with observed SST from 1930 to 2000 (Giannini et al. 2003) is at the core of our investigation. Additional integrations aid in the assessment of the roles of land–atmosphere interaction (the "fixed-β" integration), and of the SST patterns statistically related to the recent trend in Sahel rainfall (the "Sahel" integrations). The reader is referred to Section 2 and Table 1 for details on the model and integrations.

The dominant patterns of African rainfall variability during northern summer appear to be united in their common, ocean-forced nature, but distinct in that one pattern, representing the Gulf of Guinea coast, is inextricably tied to the oceanic Intertropical Convergence Zone (ITCZ), while the other, representing the Sahel, defines the continental monsoon. Lebel et al. (2003) and Gu and Adler (2004) have similarly argued for a dynamical differentiation at intra-seasonal time scales between the character of convection along the Gulf of Guinea, at 5°N, and across the Sahel, at 15°N, with a "jump" occurring between the two—from the Gulf of Guinea poleward into the Sahel—in June.

While observational studies in the 1970s and early 1980s emphasized the role of tropical Atlantic SSTs (Hastenrath and Lamb 1977; Lamb 1978a, 1978b; Lough 1986), work in the late 1980s and 1990s presented a more complex picture of African rainfall variability, with increasing evidence for the role of the tropical Pacific and Indian Oceans (Wolter 1989; Shinoda and Kawamura 1994; Rowell et al. 1995; Janicot et al. 1996; Ward 1998; Janicot et al. 2001; Rowell 2001). Since the influences of tropical Atlantic and Pacific patterns of climate variability on the African monsoon have already been discussed at length in the literature, we focus our attention on the Indian Ocean.

We are interested not simply in the role of SST anomalies as a forcing mechanism for atmospheric anomalies, but also, keeping in mind the coupled nature of Indian Ocean climate variability (Gadgil et al. 1984; Kirtman and Shukla 2002; Webster 2003; Krishna Kumar et al. 2005), in the role of persistent deep convective anomalies (Thiaw and Kumar 2001; Gadgil et al. 2003, 2004). In Section 2 we briefly describe the model and integrations performed, and the observational data used. In Section 3 we present a statistical analysis of the variability of precipitation, and covariability of surface temperature, in observations and in the model. Section 4 contains a characterization of the model's externally forced and internal modes of African climate variability. This analysis is crucial to highlighting fundamental differences between the mechanisms that control rainfall variability in the Sahel and along the Gulf of Guinea coast. Section 5 discusses the role of the Indian Ocean in the context of large-scale teleconnections and climate change. Section 6 presents some conclusions.

2 Model set-up and observational data

2.1 Model description and simulation set-up

The climate model used is NSIPP1, version 1 of the atmospheric general circulation model developed at

Table 1 Summary of integrations analyzed. Also see text and the NSIPP website, at http://nsipp.gsfc.nasa.gov

Ensemble Name	Period Covered	Ensemble Size	Specifics of Integration
AMIP	1930–2000	9	forced w/observed SSTs, 2°lat × 2.5°lon resolution
fixed-β	1950–1999	1	β fixed to climatology, i.e, land-atmosphere disabled
sahel	40 years	climatology	climatological SSTs
	"	positive	SST pattern from Fig.4b of Giannini et al (2003) added
	"	negative	same SST pattern as above subtracted from climatology

NASA's Goddard Space Flight Center in the framework of the Seasonal to Interannual Prediction Project (NSIPP) (Bacmeister et al. 2001; Giannini et al. 2003; Schubert et al. 2004). The dynamical core uses a finite-difference scheme (Suarez and Takacs 1995), convection is of the relaxed Arakawa–Schubert type (Moorthi and Suarez 1992), and the land surface model is Mosaic (Koster and Suarez 1992). Details of the model and integrations can be found at http://nsipp.gsfc.nasa.gov and in Table 1.

A nine-member "AMIP ensemble", so called in deference to the "Atmospheric Model Intercomparison Project" (Gates et al. 1998), is at the core of our analysis. It was integrated with a horizontal resolution of 2° in latitude by 2.5° in longitude, and 34 levels in the vertical in a standard σ coordinate. Each ensemble member was forced with different initial atmospheric conditions, but the same observed history of SST and sea ice. A medley of Hadley Centre, GISST, and Reynolds and Smith products (Rayner et al. 1996, 2003; Reynolds and Smith 1994) was used over the sub-periods 1930–1948, 1949–1981, and 1982–2000, respectively. Because it can be shown a posteriori that our analysis does not suffer from presumed step-wise changes in the boundary conditions (Giannini et al. 2003), and because we are interested in interannual to interdecadal variability, throughout this study we compute seasonal anomalies with respect to the long-term (1930–2000) mean.

In the AMIP ensemble atmospheric CO_2 concentration is held fixed at 350 ppm, and vegetation is prescribed to be seasonally varying, but interannually fixed. Hence, simulation of the persistent dry conditions of the 1970s and 1980s in the Sahel (Giannini et al. 2003) is evidence that the historical evolution of SST variability, the only temporal link between the model and real worlds, provided the dominant forcing. In the absence of an interactive dynamic vegetation model, we can only evaluate the role of vegetation indirectly. Assuming that in the Sahel land–atmosphere interaction and dynamic vegetation provide successive amplifying steps to the initial, ocean-forced precipitation anomalies (Zeng et al. 1999; Wang et al. 2004), we assess the role of land surface variables impacted by rainfall, e.g., surface temperature and evaporation, by comparing the AMIP ensemble to an integration where land–atmosphere interaction is disabled. This is done in a 50-year (1950–1999) simulation by setting the evaporation efficiency β, defined as the ratio of evaporation to potential evaporation, to its model climatological value taken from the AMIP ensemble. This integration is referred to as "fixed-β" (Koster and Suarez 1995; Koster et al. 2000).

Finally, in light of the results of Giannini et al. (2003), additional integrations were performed, to test the reproducibility of the relationship between the SST pattern associated with the interdecadal variability of Sahel rainfall, and rainfall itself. In this "Sahel ensemble" NSIPP1 was run for 40 years in a control simulation with climatological SSTs, and for 40 years each in two simulations in which the anomaly pattern statistically associated with the interdecadal variability of Sahel rainfall is superimposed on climatological SSTs, once with positive and once negative values. This pattern (Fig. 4b of Giannini et al. (2003)) is characterized by significant loadings in the South Atlantic and Indian Oceans, in contrast to very weak loadings in the Pacific and North Atlantic Oceans.

2.2 Climate observations over tropical Africa; validation of the precipitation climatology

Two precipitation datasets are used to validate model output. The seasonal climatology and variability of the model's northern summer (July–September, or JAS) rainfall in the tropical Atlantic basin are compared to the National Oceanic and Atmospheric Administration (NOAA)'s Climate Prediction Center (CPC) Merged Analysis of Precipitation (CMAP) of Xie and Arkin (1997), a product that synthesizes satellite and ground-based information and therefore has global coverage. Because CMAP only covers the last 20 years or so on record, to validate the long-term variability we revert to station records of accumulated monthly rainfall from the NOAA Global Historical Climate Network (GHCN) (Vose et al. 1992; Peterson and Easterling 1994; Easterling et al. 1996; see the NOAA National Climatic Data Center (NCDC) website at http://lwf.ncdc.noaa.gov/oa/ncdc.html).

Fifty seven stations in tropical Africa, between 20°S and 20°N, 20°W, and 40°E, were chosen in view of the completeness of their precipitation records during northern summer of 1930–2000.

Surface air temperature data from the same tropical African region is briefly used in Section 3.2. This data was also obtained from NOAA via the International Research Institute (IRI) for climate prediction's Data Library (http://iridl.ldeo.columbia.edu/). A smaller number of stations (44) has complete seasonally averaged records of surface air temperature, and only for the 1951–1990 period. Analysis in Section 3.2 is limited to these records.

In Fig. 1 the CMAP climatology during the July–September African monsoon season is compared to the model ensemble mean precipitation over the common period, 1979–1999. The model reproduces the correct magnitude and spatial pattern over Africa in the climatology, though it has a wet bias over the Caribbean/Central American region, and over the southwestern tip of the Arabian Peninsula. Climatology and variability in the model are underestimated in the two regional maxima, over the Cameroon highlands, and over the Guinean highlands stretching west into the Atlantic marine ITCZ. Variability in general is muted in the model, but overall the model seems to balance variability in oceanic and continental precipitation in a way that compares favorably with observations.

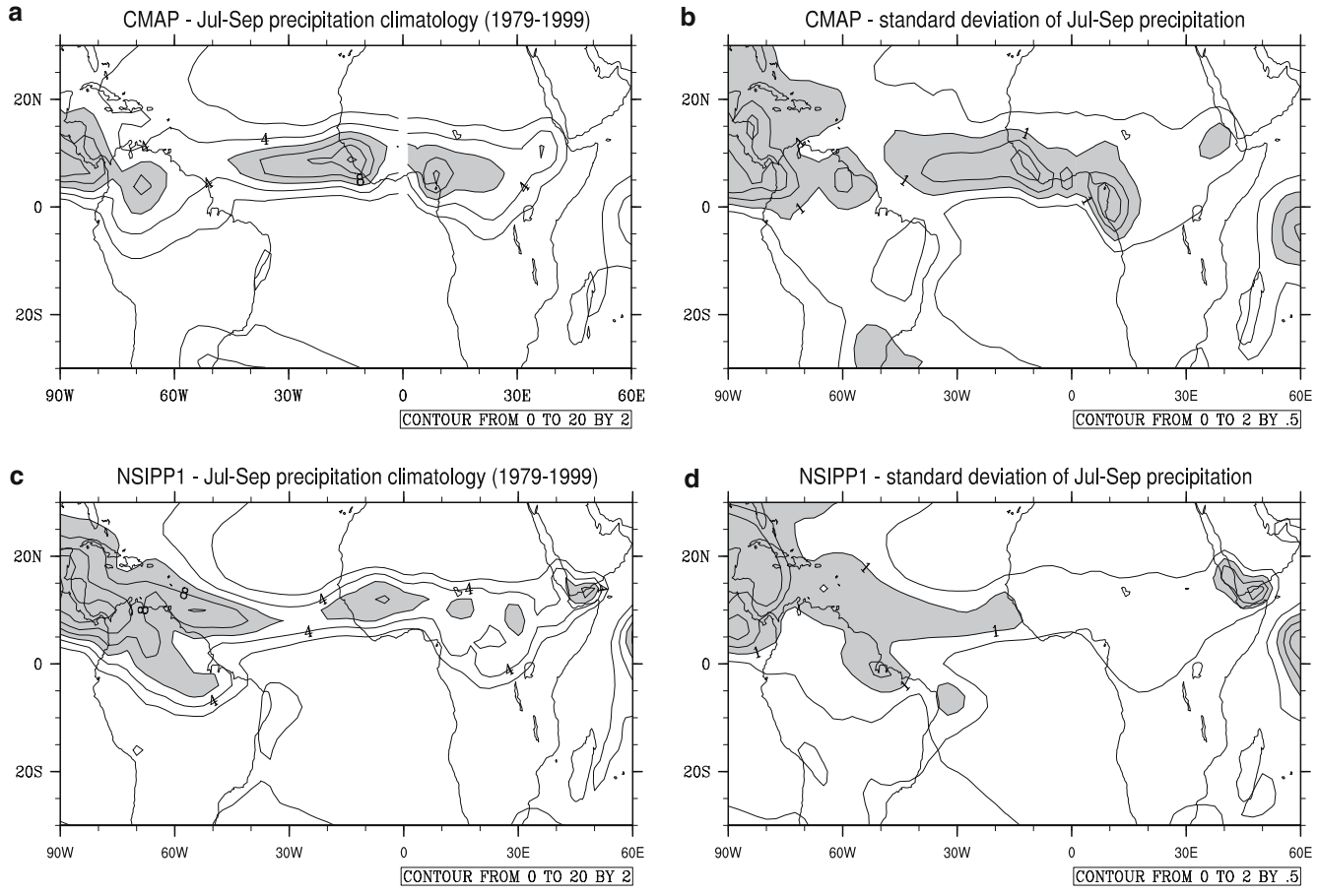

Fig. 1 Comparison of the observed (CMAP, Xie and Arkin 1997) and modeled precipitation climatologies for the July–September season (1979–1999). *Top panels* are for observations, *bottom panels* are for model output (in mm/day). Contour interval in the *left panels* is 2 mm/day, in the *right panels* it is 0.5 mm/day

3 A descriptive analysis of African climate variability (1930–2000)

To describe climate variability over tropical Africa (20°S to 20°N, 20°W to 40°E) during the northern summer monsoon season (July–September, or JAS) we use Principal Component Analysis (PCA; Preisendorfer 1988; Peixoto and Oort 1992; Von Storch and Zwiers 1999). This mathematical procedure is commonly applied to geophysical data to extract spatially coherent patterns, also known as Empirical Orthogonal Functions (EOFs) that sequentially maximize the fraction of total variability that they represent. In this section we compare results of PCA applied to precipitation (also see Giannini et al. 2003) and to surface temperature, in observations and in the ensemble mean of all integrations. In the following section the same technique will be applied to intra-ensemble member variability in rainfall.

3.1 Variability in northern summer precipitation

Figure 2 compares the two leading spatial structures, or Empirical Orthogonal Functions (EOFs) of precipitation, in observations and in the model's ensemble mean. These patterns explain 25 and 15% of the total variance in observations, 32 and 21% of the total variance in the model's ensemble mean. Panels (a) and (d) in Fig. 2 represent the observed spatial structures, with each dot depicting the loading at a station. Panels (b) and (e) represent the model ensemble-mean spatial structures. Note that the two leading model patterns represent variability at the northern and southern edges of the climatological precipitation pattern, depicted in contours.

EOF1 in observations and EOF2 in the model's ensemble mean (Fig. 2, panels a and b) represent variability in continental precipitation between 10°N and 20°N. The zonally elongated pattern of positive loadings centered on 15°N across northern Africa, from the Atlantic Ocean to the Red Sea, defines the Sahel. The regression of the associated model time series, or Principal Component (PC), with global precipitation, in Fig. 2c, shows the continental nature of the Sahel pattern. It also shows a coherent pattern of out-of-phase variation between precipitation anomalies in the central and eastern equatorial Pacific, typical of the El Niño-Southern Oscillation (ENSO) phenomenon, and in

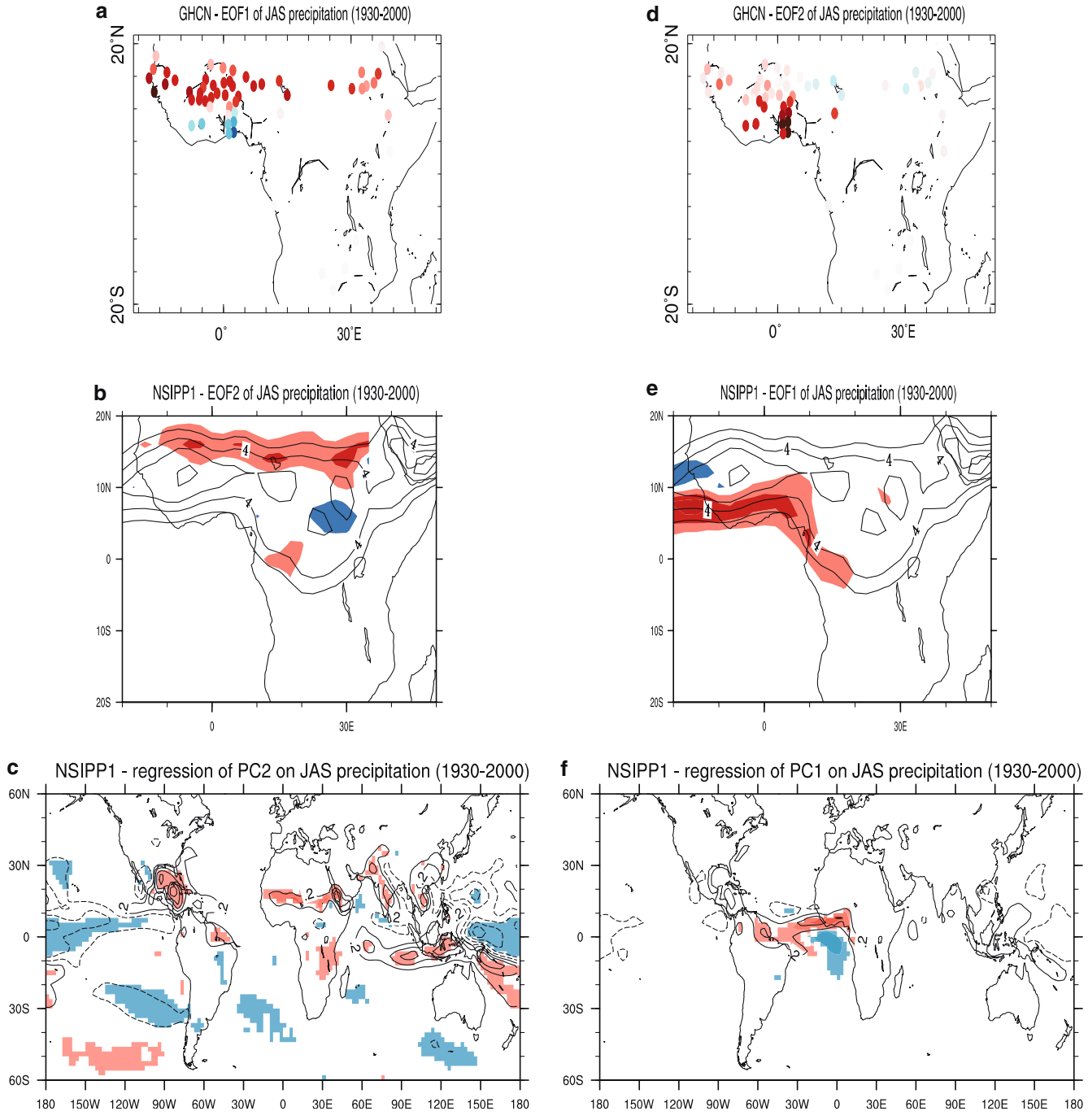

Fig. 2 The spatial patterns associated with the leading Principal Components (PCs) of northern summer precipitation variability over tropical Africa. Anomalies are in mm/day. *Top panels:* EOFs 1 and 2 from observations (stations from NOAA/GHCN)—*blue dots* represent negative anomalies, *red dots* positive anomalies. *Middle panels:* EOFs 2 and 1 of the ensemble mean of the NSIPP1 AMIP ensemble average of nine integrations—*red* is for positive anomalies, *blue* for negative anomalies. The contours, every 2 mm/day, represent the precipitation climatology (1930–2000). Note that the model PCA domain is slightly smaller in longitudinal range. It extends to 35°E, instead of 40°E, to avoid giving too much weight to the spurious maximum in simulated precipitation between the Horn of Africa and the Arabian Peninsula. *Bottom panels:* regression maps of the model PCs with global precipitation, in mm/day, with contour every 0.4 starting at 0.2, and *shading* representing statistical significance at the 99.9% confidence level

many of the world's monsoon regions. We will come back to this pattern in Section 5.

EOF2 in observations and EOF1 in the model (Fig. 2, panels d and e) represent rainfall variability along the Gulf of Guinea coast. It should be noted here that northern summer defines a relative minimum in the seasonal cycle of precipitation for this region, caught between the maxima in northern spring and fall. Nevertheless, the Gulf of Guinea coast being more humid in the mean, it exhibits a significant amount of variability

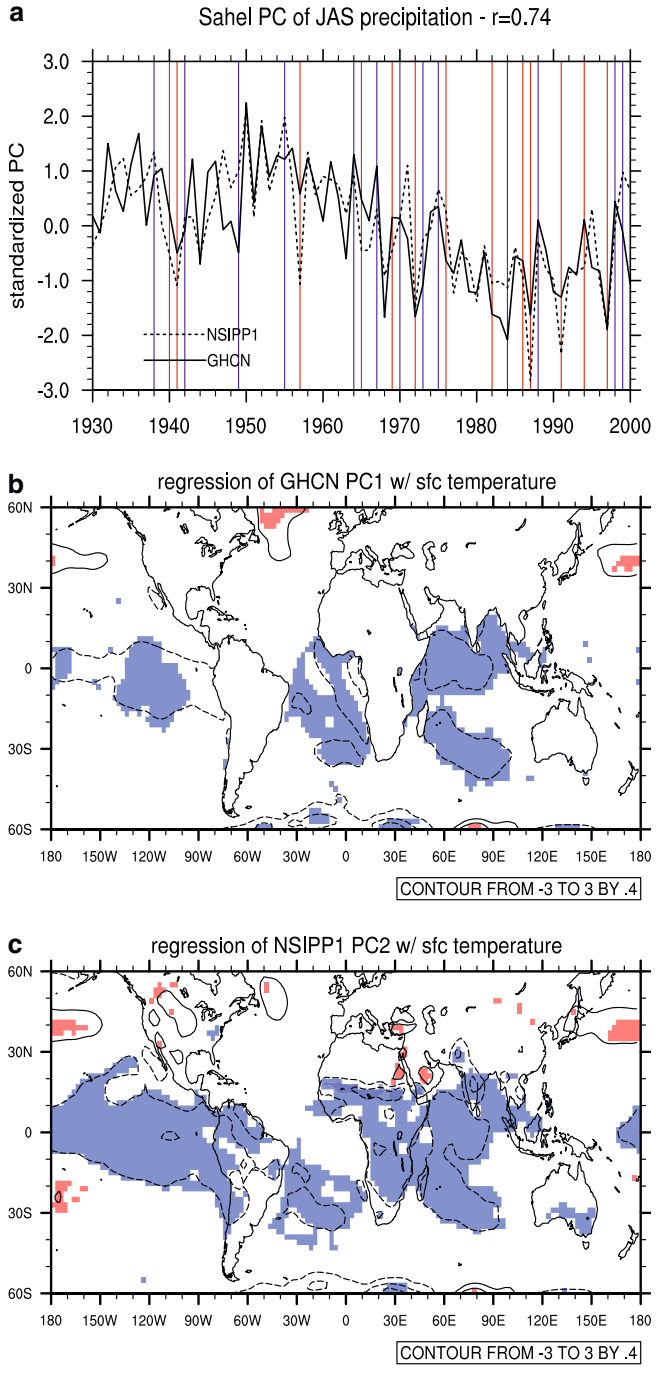

Fig. 3 The Sahel, or monsoon PC. Time series in the *top panel* are normalized (see text for additional information). The *vertical lines* identify warm (*red*) and cold (*blue*) ENSO events. Panels (**b**) and (**c**) are regression maps with surface temperature (in °C) for the observed PC1 and modeled PC2, respectively (the two correlate at 0.74 over 1930–2000). Contour interval is every 0.4°C, starting at 0.2°C, *solid contours* represent positive anomalies, *dashed contours* negative anomalies, and *shading* represents the 99.9% confidence level

even in the relatively dry summer season, appropriately captured by this EOF. As shown in the regression pattern of the associated model PC with global precipitation, in Fig. 2f, this structure connects the Gulf of Guinea coast to the tropical Atlantic Ocean ITCZ, west of our domain of analysis, covering West Africa in the latitudinal band between the equator and 10°N.

The fact that the two leading patterns appear in reverse order in the analysis of observed and modeled precipitation may be related to the inhomogeneous spatial distribution of the stations used. Because PCA is computed on the covariance, not on the correlation matrix, given that the variance in observed precipitation is higher along the Gulf of Guinea than it is across the Sahel (Fig. 1c), a Gulf of Guinea pattern should dominate. Possibly because there are fewer stations in this region, though, their coherent variability does not capture as large a fraction of the total variability as it does in the model ensemble mean.

Careful inspection of Fig. 2a reveals the presence of a meridional dipole structure in the observed Sahel pattern, between the positive loadings in the Sahel and the negative loadings along the Gulf of Guinea coast (Janicot 1992; Nicholson and Palao 1993; Rowell et al. 1995). Such a pattern is absent in the model ensemble mean figure (Fig. 2b). Its reproduction has long been considered a benchmark test for the models' ability to correctly simulate variability in the West African monsoon (e.g., Vizy and Cook 2001, 2002). Is NSIPP1's failure to reproduce this feature a model shortcoming, possibly related to inadequate spatial resolution? Awaiting a conclusive answer, we present evidence that may point, instead, to the artificial nature of the dipolar pattern. Further analysis reveals that the first EOF of observed rainfall represents a large fraction of variability in Sahel stations, not so in Gulf of Guinea coast stations, as measured by linear correlation. Correlations between the time series associated with the Sahel EOF and each station (not shown) are high and statistically significant between 10°N and 20°N, not so equatorward of 10°N. Furthermore, the correlation between the averages of Sahel and Gulf of Guinea stations is insignificant ($r = -0.05$ over July–September 1930–2000). We will come back to this distinction between Sahel and Gulf of Guinea coast patterns later in this paper, to propose that it has dynamical substance; in Section 4 we will show that the two patterns behave differently with regards to the role that boundary forcing and internal noise play in their definition.

The temporal structures of precipitation variability, or Principal Components (PCs), are shown in panels (a) of Figs. 3 and 4. The two leading PCs are statistically separate, according to North et al.'s (1982) rule, in observations and model output. The Sahel and Gulf of Guinea PCs in observations and in the model correlate at 0.74 and 0.62, respectively, over 1930–2000.

The Sahel PC (Fig. 3a) tracks the well-known "trend": precipitation was above-average in the 1930s, it hovered around the long-term mean in the 1940s, was well above it in the 1950s and early 1960s, and then progressively declined through the 1970s and 1980s. In the model time series the reversed trend, of increasing

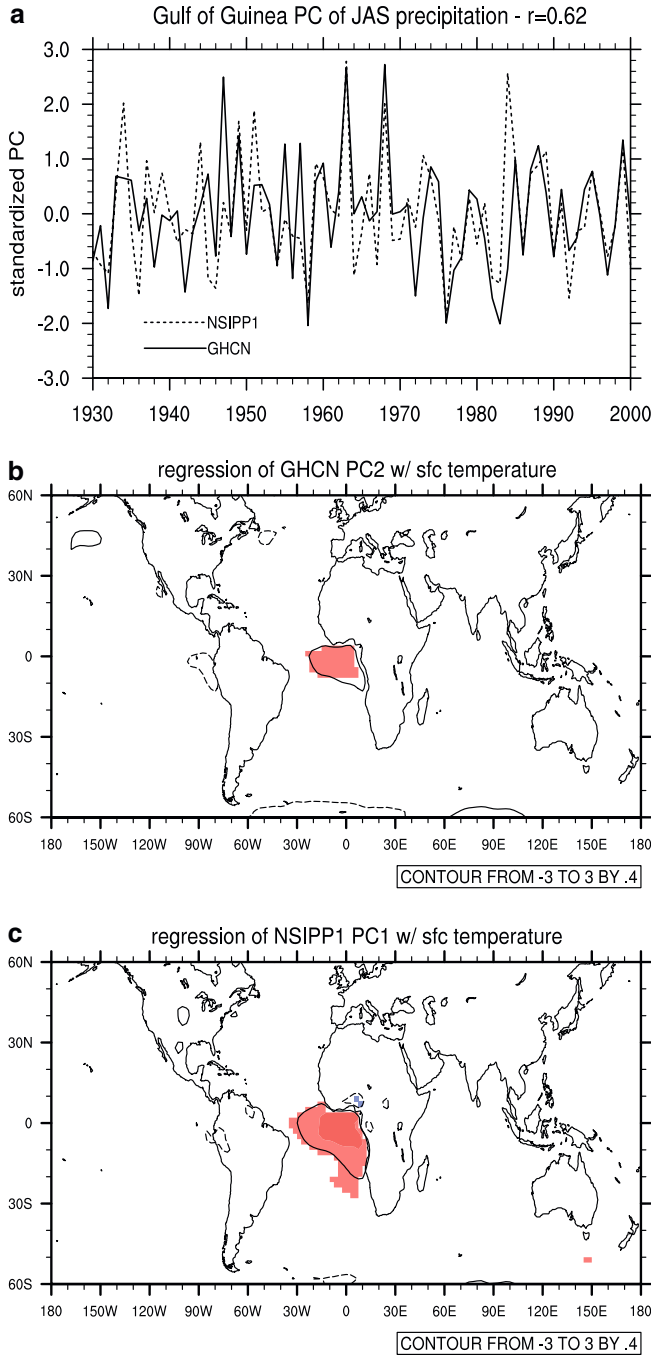

Fig. 4 The Gulf of Guinea, or oceanic ITCZ PC. Time series in the *top panel* are normalized. Panels (**b**) and (**c**) are regression maps with surface temperature (in °C) for the observed PC2 and modeled PC1, respectively (the two correlate at 0.62 over 1930–2000). *Contour* and *shading* as in Fig. 3

precipitation from the late 1980s onwards, is accentuated compared to observations. It should be noted here that the comparison between observed and model ensemble mean PCs benefits from standardization of the time series, i.e., the original time series are divided by their respective singular values (or, equivalently, by the square root of their respective eigenvalues). This is because variability in the model is muted with respect to observations, as mentioned in Section 2.2. In the case of the Sahel PCs, the ratio of observed to model ensemble mean singular values is 4. Regression maps of the Sahel PC with surface temperature are displayed in panels (b) and (c) of Fig. 3, for observations and model output, respectively. Regions of highly significant values (the shading in Figs. 3 and 4 represents statistical significance at the 99.9% level) span the entire tropical oceans. In the case of the model PC (Fig. 3c), the regression includes the simulated, ensemble-mean surface temperature over land: significant regression values can be noted over the Indian subcontinent and across the Sahel itself.

The Gulf of Guinea PC is shown in Fig. 4a. No trend is apparent in this time series, an indication that PCA has successfully confined it, and hopefully its physics, to the complementary leading mode. In Fig. 4, panels (b) and (c) display the regression maps of this PC with surface temperature, in observations and model, respectively. The very different nature of this pattern, when compared to that associated with the Sahel PC, is immediately apparent: high positive regression values are localized to the eastern equatorial Atlantic, in the region of SST variability associated with the Atlantic counterpart to the tropical Pacific ENSO.

3.2 Co-variability in surface temperature

The comparison of the leading PCs of the model's ensemble mean surface temperature and precipitation (Fig. 5), calculated independently over the same region (20°S to 20°N, 20°W to 35°E), reveals the coherence in their variations. The two leading patterns of ensemble-mean surface temperature explain 53 and 17% of the total variance, respectively. Though obtained independently, they correlate at 0.91 and 0.81 with the corresponding leading PCs of precipitation, in reverse order: PC1 of model ensemble-mean surface temperature is a Sahel/continental pattern, related to PC2 of precipitation, while PC2 of surface temperature is a Gulf of Guinea/oceanic pattern, related to PC1 of precipitation.

Values of opposite sign in the spatial patterns associated with the continental PCs of precipitation and surface temperature (panel b of Figs. 2 and 5, respectively) represent trends of contrasting sign across the Sahel: as precipitation decreased over the past 50 years, surface temperature increased. The coupling of trends of opposite sign in precipitation and surface temperature in the Sahel is confirmed by a repeat of PCA on station surface air temperature data (not shown). The first PCs of observed precipitation and surface air temperature correlate at 0.82 during 1951–1990—analysis is limited to this sub-period due to the temporal limitation of the surface air temperature records available from GHCN. PC1 of observed temperature explains 39% of the total variance over Africa, 20°S to 20°N. Again, high spatial loadings (not shown) are focused on the Sahel, 10°N to 20°N.

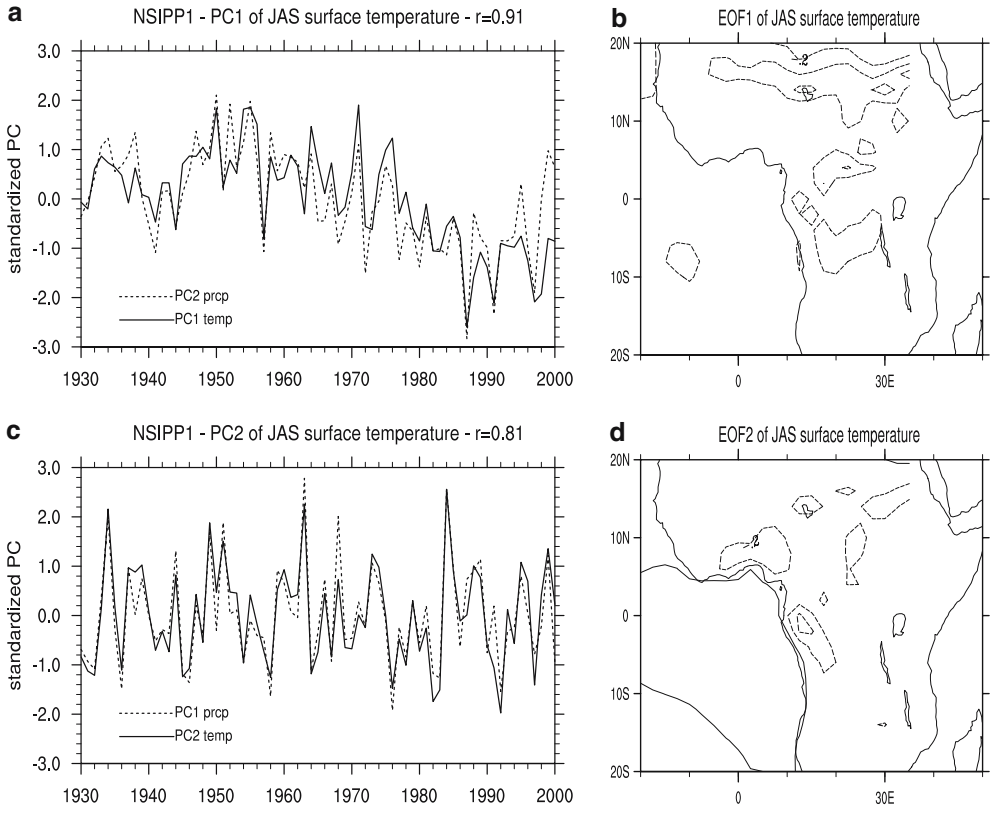

Fig. 5 PCA of the ensemble-mean surface temperature in the NSIPP1 AMIP ensemble. *Left column:* the PCs are normalized. *Solid lines* are the PCs of surface temperature, *dashed lines* the PCs of precipitation. *Right column:* contour is every 0.2°C, *solid contours* represent positive anomalies, *dashed contours* negative anomalies

While over the tropical oceans surface temperature and precipitation tend to be positively correlated, i.e., precipitation is usually largest over the warmest SSTs, the opposite is true over land. Over land the surface temperature signal is most directly interpretable as a consequence of the precipitation signal: increased precipitation is associated with increased soil moisture, which means that a given energy flux into the surface will be used preferentially to evaporate the moisture, rather than to heat the surface. A negative short-wave cloud feedback is also consistent with an out-of phase relationship between precipitation and surface temperature anomalies: the cloud cover associated with rainfall reduces the incoming solar radiation at the surface, leading to surface cooling. Regression plots of the Sahel PC of precipitation with precipitation, evaporation and vertically integrated moisture convergence (Lenters and Cook 1995; Vizy and Cook 2001) from the AMIP ensemble (left column of Fig. 6) demonstrate that local and large-scale processes contribute to the water budget in comparable parts. Once a precipitation anomaly, in our case remotely forced from the ocean, is established (Fig. 6a), local moisture recycling, represented by the evaporation anomaly (Fig. 6c), and large-scale dynamical constraints, represented by the moisture convergence anomaly (Fig. 6d), contribute in equally significant terms to precipitation across Africa.

When land–atmosphere interaction is severed, in the fixed-β integration (right column of Fig. 6), the anomalous precipitation (Fig. 6e) does not result in surface temperature (Fig. 6f) or evaporation (Fig. 6g) anomalies as large or significant as in the AMIP ensemble. Note that the fact that surface temperature anomalies across the Sahel in fixed-β are a fraction of the corresponding AMIP ensemble anomalies implies that evaporation plays a dominant role in defining surface temperature, compared to cloud-radiative feedbacks. The fact that the surface temperature anomalies are negative implies that the short-wave cloud feedback, i.e., cooling by a reduction of incoming solar radiation at the surface, wins over the long-wave cloud feedback, which would result in more energy being trapped below the clouds, hence a warming.

The opposite sign in anomalies in precipitation and land surface temperature is confirmed in the modeled Gulf of Guinea patterns. The correlation between these EOFs of precipitation and surface temperature (compare panel d in Fig. 5 with panel e in Fig. 2) reflects the association between anomalies of the same sign in precipitation and Gulf of Guinea SST, and of opposite sign in precipitation and land surface temperature along the Gulf of Guinea coast. For a discussion of the dynamics involved in the forcing of an anomalous atmospheric circulation by eastern equatorial Atlantic SSTs the reader is referred to the comprehensive modeling studies of Vizy and Cook (2001, 2002).

In brief, the following points summarize what described so far:

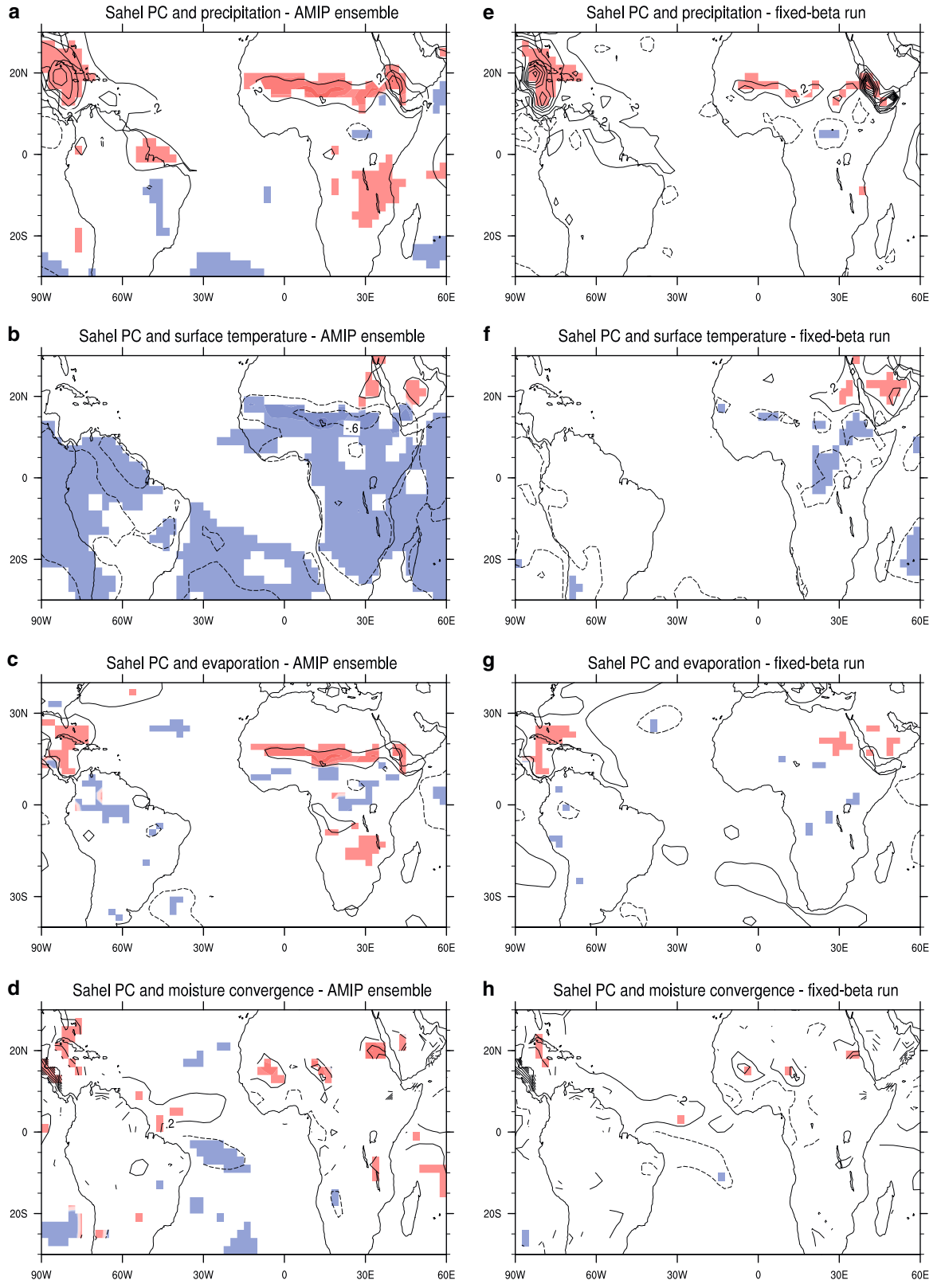

Fig. 6 Regression maps of the Sahel PC with (**a**–**e**) precipitation, (**b**–**f**) surface temperature, (**c**–**g**) evaporation, and (**d**–**h**) vertically integrated moisture convergence, from the AMIP ensemble (*left column*), and from the fixed-β run (*right column*). **a**–**e** are in units of mm/day, (**b**–**f**) are in °C, (**c**–**g**) and (**d**–**h**) are in mm/day. In (**a**–**e**), (**b**–**f**), and (**d**–**h**) contour is every 0.4, starting at 0.2. In (**c**–**g**) contour is every 0.2, starting at 0.1. *Solid contours* denote positive anomalies, *dashed contours* negative anomalies, and *shading* indicates the 99.9% confidence level

1. When forced with the historical record of SST only, NSIPP1 skillfully captures the observed interannual to interdecadal variability of northern summer African climate. This includes the interdecadal drying trend in the Sahel, and interannual variability typical of Gulf of Guinea rainfall.
2. The observed relationship between precipitation and land surface temperature in the Sahel, while consistently reproduced in the AMIP ensemble, vanishes in an integration where land–atmosphere interaction is disabled. This behavior is suggestive of a strong control exercised by precipitation on surface temperature through a land–atmosphere feedback. As a corollary, the positive trend in Sahel surface temperature can be interpreted as a consequence of the negative trend in precipitation.

4 Signal and noise in the modeled African monsoon

Having shown that the model is capable of capturing the dominant patterns of the observed variability of precipitation, and that such patterns owe their existence primarily to SST forcing, next we exploit the information contained in the ensemble of integrations to further investigate the nature of such patterns. We are interested in discriminating between signal and noise in African rainfall variability as a first step towards quantifying potential predictability.

We define the signal as the boundary-forced component, while the noise is variability internal to the atmosphere, or to the coupled land–atmosphere system, which is independent of the prescribed oceanic boundary conditions. Assuming linearity, Zwiers (1996), Rowell (1998), and Koster et al. (2000), among others, write:

$$\sigma^2_{\mathrm{Total}} = \sigma^2_{\mathrm{Forced}} + \sigma^2_{\mathrm{Internal}}$$

where σ^2 is variance. "Forced" refers to boundary forcing from the prescribed oceanic conditions. In the limit of infinitely large ensemble size, the "Forced" component of variability is represented by the time-varying ensemble mean, while the "Internal" component of the variance, i.e., that due to atmospheric noise and/or variability arising from land–atmosphere interaction, is represented by deviations from it.

We apply PCA to total and internal variability of precipitation over Africa, 20°S to 20°N and 20°W to 35°E, as we did to forced variability in the previous section. The percent variances explained by the leading PCs of forced, total and internal variability are summarized in Table 2.

PCA is first repeated on the total variability of precipitation as represented by the "stack" of deviations of all the ensemble members from the ensemble's July–September precipitation climatology. Results are displayed in Table 2 and in Fig. 7. The two leading spatial patterns are indistinguishable from those of ensemble-mean (Fig. 2, panels b and e), or forced variability, hence they are not shown. EOF1 is a Gulf of Guinea pattern, explaining 19% of the total variance. EOF2 is a Sahel pattern, explaining 15% of the total variance. Note that the percent variances explained by the two leading PCs of total variability, in the first column of Table 2, compare well with the percentages explained by the observed PCs 1 and 2 of precipitation, of 25 and 15%, respectively, over 1930–2000. Also note, in Fig. 7b, that all the ensemble members reproduce the trend in Sahel rainfall. Correlation values of the ensemble-mean PCs 1 and 2 with the individual ensemble-member realizations range between 0.94 and 0.96 in PC1, the Gulf of Guinea PC, and between 0.84 and 0.89 in PC2, the Sahel PC. From visual inspection alone, it is clear that the scatter between individual realizations of the model's Gulf of Guinea PC is smaller than that between individual realizations of the Sahel PC (compare panels in Fig. 7). Following Koster et al. (2000), to measure the tightness of the spread, or coherence among realizations we compute:

Table 2 Percent variances explained by the leading PCs of the total, forced, and internal components of variability in the AMIP integrations. Ω, the coherence reported in the fourth column, is computed using the total and forced components of variability. See text for details

	σ^2_{Total}	σ^2_{Forced}	Ω	$\sigma^2_{Internal}$
Gulf of Guinea PC	19%	32%	0.91	–
Sahel PC	15%	21%	0.70	10%

$$\Omega = \frac{I\sigma^2_{\mathrm{Forced}} - \sigma^2_{\mathrm{Total}}}{(I-1)\sigma^2_{\mathrm{Total}}}$$

where I is ensemble size. Ω can take values between 0 and 1. Where the I realizations to display variability completely independently of each other, then, from the Central Limit Theorem it would follow that $\sigma^2_{\mathrm{Forced}} = \sigma^2_{\mathrm{Total}}/I$, hence $\Omega = 0$. Conversely, were the I realizations to all display the same variability, then $\sigma^2_{\mathrm{Forced}} = \sigma^2_{\mathrm{Total}}$, hence $\Omega = 1$. In both our PCs, the coherence among realizations is high, as seen in values of Ω of 0.91 and 0.70 in Table 2. As expected, coherence is higher for the Gulf of Guinea PC than for the Sahel PC.

Not surprisingly, then, in the repeat of PCA on the internal variability of rainfall, i.e., on the deviations of each and every ensemble member from the time-varying ensemble mean (Table 2 and Fig. 8), we find that the dominant pattern of forced and total variability, the Gulf of Guinea pattern, is no longer a preferred pattern. Instead, the dominant pattern of internal variability (Fig. 8), explaining 10% of the total variance of precipitation, is continental, bearing a strong resemblance to the Sahel pattern. From a statistical standpoint, this finding is consistent with the noise level in the individual ensemble members of the two leading PCs being higher for the Sahel than for the Gulf of Guinea, as noted above in relation to the scatter in the time series in Fig. 7. Similar results have recently been obtained by

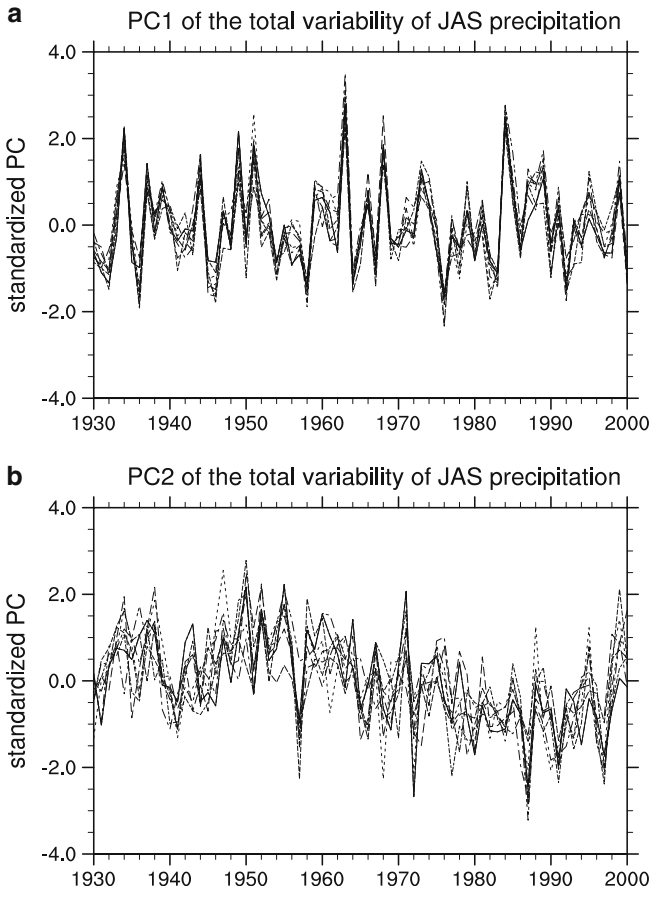

Fig. 7 PCA of the total variance of July–September precipitation over tropical Africa. **a** Time series for each ensemble member associated with a Gulf of Guinea pattern. **b** Time series associated with a Sahel pattern. The amplitude is in units of standard deviation

Tippett and Giannini (2005), who analyzed the predictable components of West African rainfall in a different atmospheric model. More relevant is the dynamical interpretation this behavior lends itself to; Gulf of Guinea and Sahel patterns represent two different mechanisms of rainfall variability over West Africa, with distinct spatial and temporal scales, as seen in Section 3, and controls. The Gulf of Guinea pattern owes its existence entirely to SST variability, more precisely to tropical Atlantic SST variability. The Sahel pattern is continental in nature, and displays a significant amount of noise which is amplified by land–atmosphere interaction (see previous section and Fig. 6; also see Fig. 3 in Giannini et al. (2003)). Because very similar spatial patterns appear among the leading modes of boundary-forced and internal variability, and because the amplitude exhibited by the boundary-forced Sahel pattern is larger than that exhibited by its internal variability counterpart (the ratio of Sahel eigenvalues of boundary-forced and internal variability is 3), we interpret the Sahel pattern as an internal mode of variability of northern summer African precipitation, a mode in which land–atmosphere interaction matters, and that is preferentially excited and amplified by SST variability.

5 Dynamics of the Indian Ocean–Sahel teleconnection

Over the past 30 years research into the linkages between the world's oceans and the persistence of drought in the Sahel has expanded from a focus on the tropical Atlantic (e.g., Hastenrath and Lamb 1977; Lamb 1978a, 1978b) to include the Pacific (e.g., Folland et al. 1986; Palmer 1986; Wolter 1989; Janicot et al. 1996), and Indian Oceans (Shinoda and Kawamura 1994; Janicot et al. 2001; Rowell 2001). In this section we describe three plausible dynamical mechanisms that may explain the link between a warming trend in the tropical oceans and the drying of the Sahel (Bader and Latif 2003; Giannini et al. 2003). These three mechanisms are closely inter-related, and could be portrayed as three levels of increasing complexity in the atmospheric response to SST anomalies, rather than three independent, competing mechanisms. The first mechanism involves the thermal contrast between land and ocean. Its consideration follows from a study of Chou et al. (2001) on idealized monsoons. The second mechanism relates to zonally

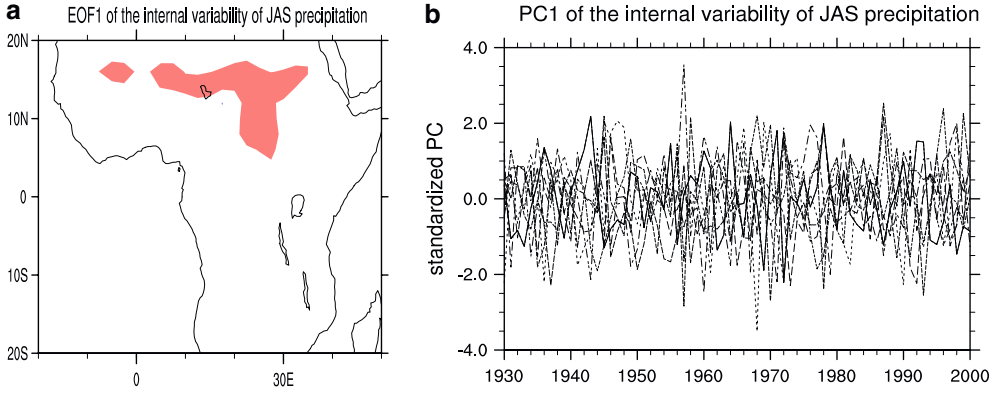

Fig. 8 PCA of the internal variance of July–September precipitation over tropical Africa. The leading pattern represents noise in a Sahel-like pattern. The amplitude for the time series is in units of standard deviation

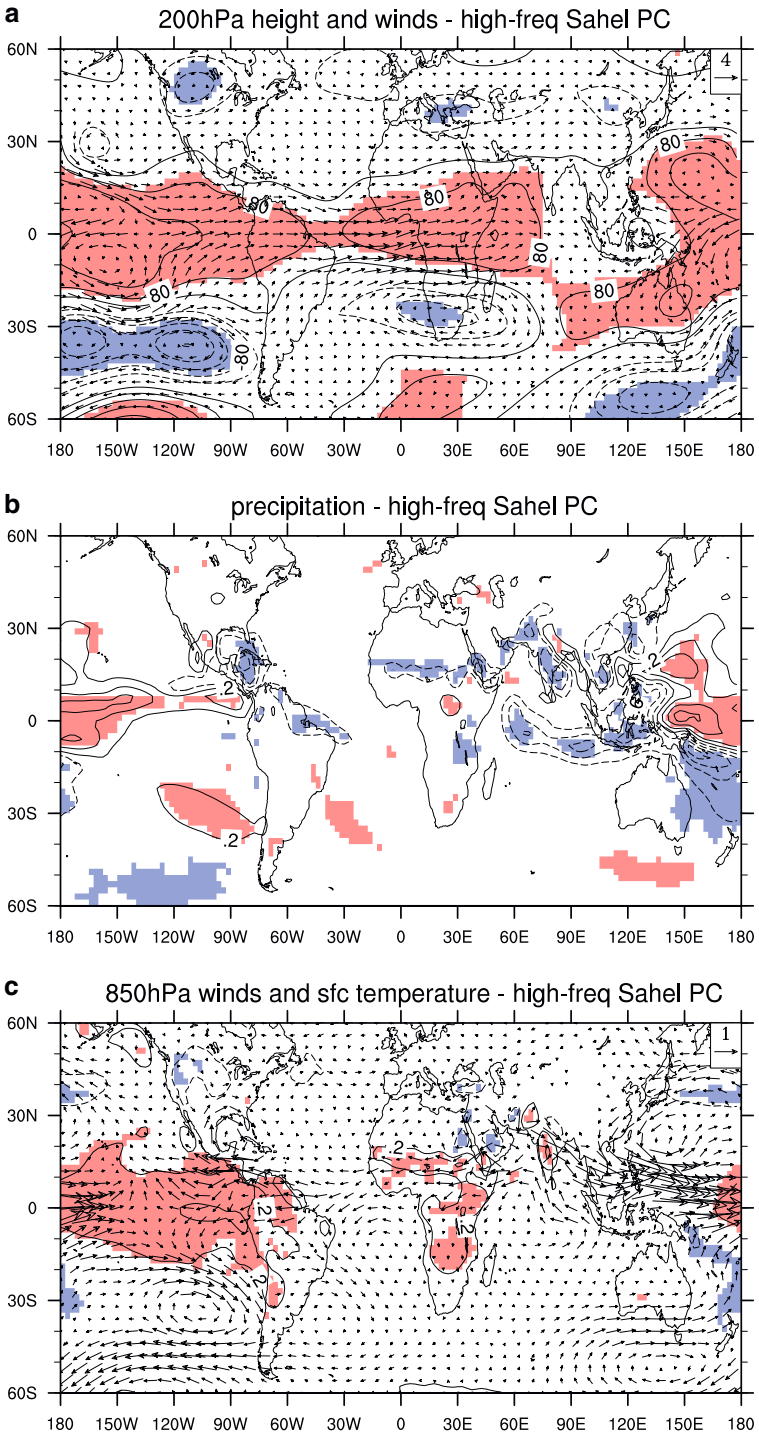

Fig. 9 Regression maps of the high-frequency component of the Sahel PC with (**a**) 200 hPa geopotential height (contour every 40 gpm) and winds, (**b**) precipitation (contour every 0.4 mm/day, starting at 0.2), (**c**) 850 hPa winds and surface temperature (contour every 0.4°C, starting at 0.2). *Solid contours* denote positive anomalies, *dashed contours* negative anomalies, and *shading* indicates the 99.9% confidence level

symmetric atmospheric dynamics involving the global Hadley circulation. The third mechanism, the eddy response to localized heating, interprets deviations from the global Hadley circulation in light of the theory of equatorial wave dynamics (Matsuno 1966; Webster 1972; Gill 1980).

The starting point of our analysis is the decomposition of the Sahel PC of precipitation (Fig. 3a) into "low-frequency", or interdecadal (21-year running mean), and "high-frequency", or interannual (its residual) components (Giannini et al. 2003; see their Fig. 4). This procedure separates the influence of the tropical Pacific and ENSO, which operates on the interannual time scale, from that of the tropical oceans around Africa. Implicit in our interpretation of this separation is the reasoning that the time scale, interannual or interdecadal, is set by the slower component of the ocean atmosphere system, i.e., the ocean, or by ocean–atmosphere interaction, as in

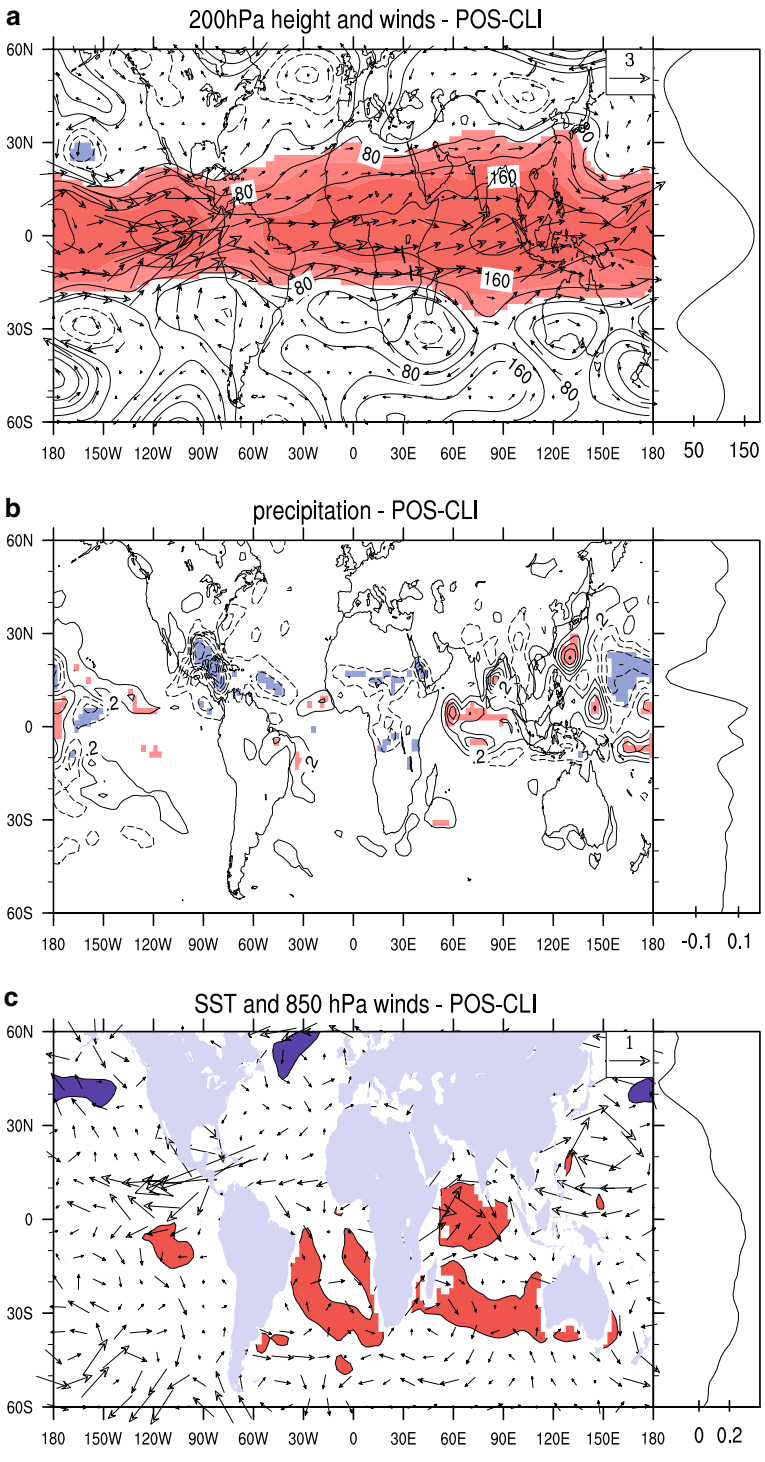

Fig. 10 Composites of the positive-climatology differences in the Sahel ensemble. **a** Geopotential height (contour is every 40 gpm) and winds at 200 hPa (in m/s), **(b)** precipitation (in mm/day—contour is every 0.4 mm/day, starting at 0.2 mm/day), and **(c)** 850 hPa winds (in m/s) and SST—in °C. Contour is every 0.4°C. *Shading* in (**a**, **b**) indicates the 99.9% confidence level. The *line plots* to the right of each panel represent the zonal mean of the variable that is contoured in the panel. In the case of surface temperature the zonal average is taken over the oceans only

ENSO. However, at any given time in the interannual or decadal "cycle" of these anomalies, the atmosphere responds to the anomalies present, with no regard to the characteristic time scale of their evolution.

Before focusing the rest of the discussion on the impact of SST variability associated with the low-frequency component of Sahel rainfall, we comment briefly on ENSO's role in shaping its interannual variability. In Fig. 9, the high-frequency component of the Sahel PC is regressed against relevant atmospheric variables. Positive SST anomalies in the tropical Pacific (Fig. 9c) are associated with positive upper-level geopotential height anomalies (Fig. 9a); in a warm ENSO, the entire tropical troposphere warms up (Yulaeva and Wallace 1994), and the vertical profile becomes more stable (Chiang and Sobel 2002; Su et al. 2004). Hence, the regions clima-

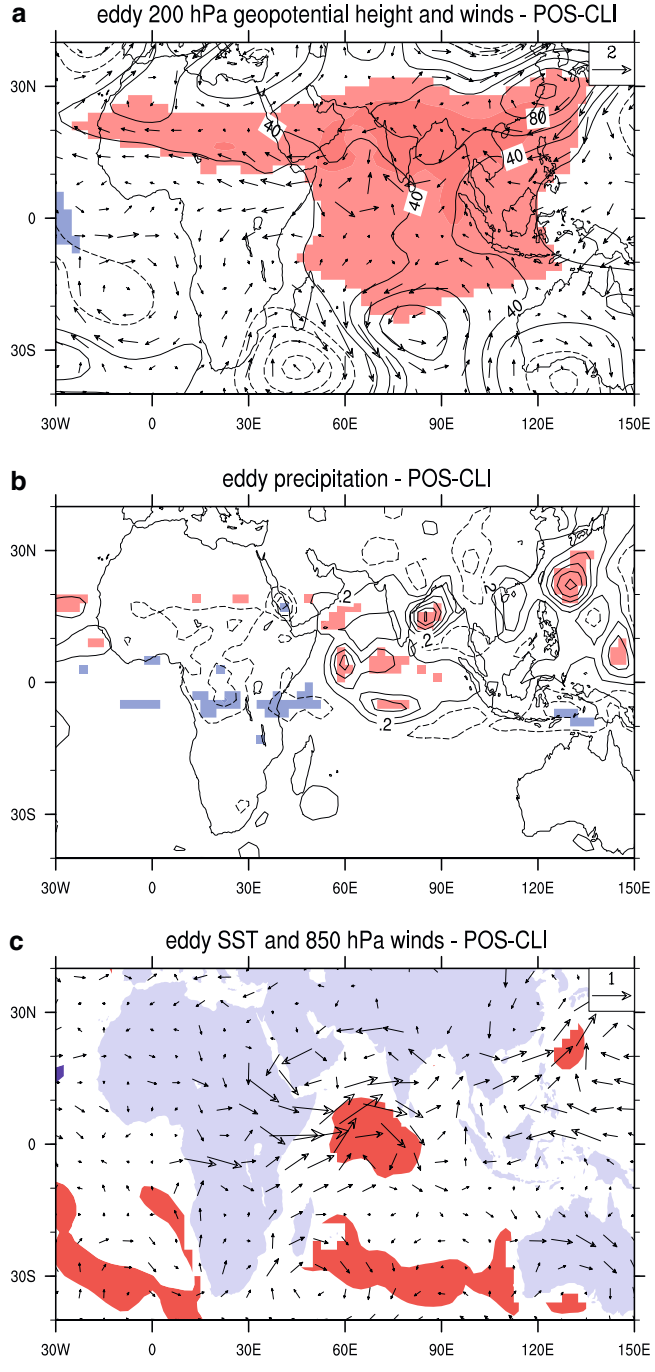

Fig. 11 As in Fig. 10, except for the zonal eddy circulation. Contour intervals are: (**a**) every 20 gpm, (**b**) every 0.4 mm/day, starting at 0.2 mm/day, (**c**) every 0.4°C, starting at 0.2°C

tologically affected by deep convection all suffer a reduction in rainfall, visible in Fig. 9b across Africa, South Asia, and Central America. Consistently, as seen in Section 3.2, as precipitation decreases, land surface temperature increases.

To describe the impact associated with the low-frequency component of Sahel rainfall we analyze the "Sahel ensemble". We designed this set of integrations specifically as a test for the dynamical consistency of the statistical relationship identified by Giannini et al. (2003), between large-scale patterns of SST and the long-term trend of Sahel rainfall. We compare a pair of 40-year integrations, referred to as "positive" and "negative" Sahel, to a 40-year climatological SST integration. The "positive" and "negative" Sahel simulations are obtained by forcing the atmospheric model with the pattern statistically related to the low-frequency variability of Sahel rainfall added or subtracted, respectively, to climatological SSTs. Linearity of the response to SST is tested, by comparing "positive minus climatology" and "negative minus climatology" differences. Since the response is found to be linear, we will only discuss the "positive minus climatology" case.

The SST anomalies in the positive Sahel integration (see Fig. 4b of Giannini et al. (2003) or Fig. 10c here) capture the net warming of the South Atlantic and Indian Oceans. The latter, according to Levitus et al. (2000), dates back to the mid-1960s. The contribution from the tropical Pacific is negligible, having been isolated into the interannual component. Also of note is the absence of significant anomalies in the North Atlantic, hence of an Atlantic interhemispheric gradient in SST, which has been argued to contribute to long-term variability of rainfall in the Sahel (Folland et al. 1986; Rotstayn and Lohmann 2002; Hoerling et al. 2004).

Before we go on to interpret the role of Indian Ocean SSTs in the Sahel simulations, we note that the validity of the AMIP framework has been called into question by observational and modeling studies which qualify the breakdown of the association between warm SST and above-average precipitation in the Indian Ocean during the southwesterly monsoon season (Rao and Goswami 1988; Kirtman and Shukla 2002; Gadgil et al. 2003; Krishna Kumar et al. 2005). In reality, warm SSTs in the Indian Ocean during northern summer are more consistently interpreted as the consequence of reduced deep convection and cloud cover, and increased incoming solar radiation at the surface, than as the cause for increased precipitation. Hence, forcing a model with SSTs can create an unrealistic source of energy and moisture, which leads to an unrealistic precipitation response. This could be, indeed, what our model simulates. Assume, on the other hand, that we could separate two components in Indian Ocean SST variability. One component would be arising from local, coupled ocean–atmosphere dynamics with strong signature on the interannual time scale. The other would be externally forced, e.g., from the radiative effect of increased atmospheric greenhouse gas concentrations, or from decadal or longer-term changes in ocean circulation, and would manifest itself in the trend. By attributing the equatorial Indian Ocean warming to the latter, externally forced mechanism, we could rightfully interpret the response in Sahel rainfall as a consequence, via the atmospheric response described above, of this externally forced trend component in the variability of Indian Ocean SSTs.

5.1 The role of land-ocean temperature contrast

In their idealized study, Chou et al. (2001) show how, in regions dominated by the monsoon, precipitation over land can be favored at the expense of oceanic precipitation. The balance ultimately involves temperature gradients, set up by the differences in heat capacity of land and ocean, and moisture availability. At equinox conditions, if the land surface is artificially saturated in moisture, there is no difference between land and ocean—equatorial convection extends across land and ocean surfaces. When soil moisture is not prescribed to be saturated, and is, instead, allowed to interact with the atmospheric circulation, oceanic convection is favored at the expense of continental convection, presumably because moisture is readily available over the ocean. Finally, when a simple parameterization of the meridional ocean heat transport is added, which effectively cools the tropical oceans by exporting heat to mid-latitudes, the continental convergence zone gains the upper hand.

In our simulations, the positive minus climatology difference equates to a warming of the tropical oceans. Composites of this difference, i.e., the difference between the July–September 40-year average in the positive Sahel and climatology integrations, in 200 hPa geopotential height and winds, precipitation, and surface temperature and 850 hPa winds are displayed top to bottom in Fig. 10. The line plots to the right of each panel represent the zonal mean of the quantities contoured in the corresponding spatial plot. These anomaly patterns are virtually indistinguishable from regression plots (not shown) of the low-frequency component of the Sahel PC on the same variables taken from the AMIP ensemble mean.

If we focus our attention on the precipitation anomalies in the positive-climatology difference (Fig. 10b), we find that concomitant with the warming of the Indian and South Atlantic Oceans, and with the drying of the Sahel, precipitation increased in the equatorial Indian Ocean. Unfortunately, due to the absence of critical station data from available archives, we are unable to confirm the relationship between long-term variability of rainfall in the Sahel and in the equatorial Indian Ocean. For example, the record from the one station in GHCN representative of the western equatorial Indian Ocean, Mahé in the Seychelles, is incomplete—data is missing for the crucial years which signaled the transition between wet and dry epochs in the Sahel, i.e., 1963–1972. However, a recent study by Hurrell et al. (2004) finds basin-wide consistency between observed and modeled trends in precipitation in the Indian Ocean.

The association between below-average rainfall in the Sahel and above-average precipitation in the equatorial Indian Ocean fits the mechanism described above: a warming of the tropical oceans, as in the idealized simulation of Chou et al. (2001) where meridional ocean heat transport is disabled, shifts convection from land to ocean. This interpretation then brings to our attention the question of attribution—why have the tropical oceans consistently warmed up in the past few decades?

5.2 The response of the Hadley circulation to an equatorial SST warming

The precipitation anomalies in the equatorial Indian Ocean (Fig. 10b) are colocated with, and of the same sign as, the SST anomalies (Fig. 10c), and are most conspicuous just to the north and to the south of the equator between 50°E and 90°E. Precipitation shows a decrease all around the globe at latitudes between 10°N and 20°N—noticeable in the zonal-mean plot to the side of Fig. 10b. The decrease is marked across the monsoonal regions of Central America and the Caribbean, in the Sahel, and over the western tropical North Pacific. In contrast, precipitation increases in the equatorial Indian Ocean, between 50°E and 110°E, in the Bay of Bengal, and in the western equatorial Pacific. These changes imprint the zonal mean picture, representative of the global Hadley circulation. We hypothesize that a warming not only of tropical SSTs, but more specifically of equatorial SSTs, warming which is especially marked in the Indian Ocean, may have favored a more equatorial position of the ascending branch of the global Hadley circulation, hence of the locus of deep convection. Near-surface and upper-level winds would then have adjusted to the newly found equilibrium between the global atmospheric circulation and the diabatic heating anomalies that perturbed it.

Positive 200 hPa geopotential height anomalies (Fig. 10a) not unlike those associated with the response to the equatorward shift of convection typical of a warm ENSO event (see Fig. 9) are consistent with an increase in equatorial deep convection in the Indian and western Pacific Oceans, with a marked center in the Indian Ocean between 60°E and 100°E. Away from the equator, the anomalies in 200 hPa winds are consistent with quasi-geostrophic flow along the geopotential height anomaly contours. Of particular interest here is the weakening of the tropical easterly jet in the region between South Asia and Africa, in the latitudinal band between 10°N and 20°N—a weaker than normal upper-level jet is a hallmark sign of years of reduced Sahel precipitation (Newell and Kidson 1984; Nicholson and Grist 2001).

5.3 The zonal eddy response and equatorial wave dynamics

An interesting degree of complexity is added when one considers deviations from the zonal mean in the atmospheric circulation (Fig. 11). Then, the eddy component of the upper-level and near-surface flows in the African–Asian sector can be interpreted as the dynamical response of the atmosphere to the superposition of two competing diabatic heat sources, one equatorial and

another off-equatorial (Webster 1972; Gill 1980). The equatorial heat source is, again, one associated with anomalously strong convection in the Indian Ocean (Fig. 11b). Consistent with Gill's (1980) description, to the west of the heat source are near-surface westerly wind anomalies converging towards it (Fig. 11c), and upper-level easterly anomalies diverging away from it (Fig. 11a). The Rossby-wave component of the response to this heat source alone would draw a northeasterly near surface flow across the Sahel, recurving to westerly at the equator, synonymous with a weakening of the southwesterly monsoon across Africa. However, the picture is complicated by the presence of off-equatorial heat sources, which represent strengthening of the monsoon, and are centered on the Bay of Bengal and in the western North Pacific. Consistently, zonal eddy 200 hPa geopotential height anomalies (Fig. 11a) are positive in a sector centered on the Bay of Bengal, from across the Sahel to East Asia. Upper-level wind anomalies capture a strengthening of the tropical easterly jet between Africa and India, while near-surface wind anomalies capture a strengthening of the South Asian monsoon. The off-equatorial heat source in the Bay of Bengal would alone draw southwesterly flow to the west of it, strengthening the African monsoon across the Sahel. In the balance, Sahel rainfall in the positive-climatology difference of the zonal eddy field (Fig. 11b) is negative, but not significantly so, compared to the total (Fig. 10b) field.

The African response to SST and precipitation in the Asian sector has potential value for understanding and predicting a new balance of forces, one that could develop with climate change. If the warming of the tropical oceans (Levitus et al. 2000) is a sign of anthropogenic climate change (Barnett 2005), will it necessarily spell doom for the Sahel and other semi-arid climates of the Earth (Neelin et al. 2003; Chou and Neelin 2004)? Or will a projected strengthening of the Asian summer monsoon, brought about by the increased land–ocean thermal contrast associated with a sped-up melting of snow cover (Meehl and Washington 1993; Krishna Kumar et al. 1999; Houghton et al. 2001), be able to counteract the drying trend?

6 Conclusions

The comparison of observations and model simulations presented here confirms the dominant role played by the oceans in African climate variability (Folland et al. 1986; Giannini et al. 2003), at least on interannual to interdecadal time scales. The picture that emerges is that of climate variability that is remotely forced from the ocean, and amplified by local land–atmosphere interaction. Vegetation and dust could conceivably play a role parallel to that of the land surface, in responding by amplifying the remotely forced precipitation anomalies (Zeng et al. 1999; Wang et al. 2004).

In this concluding section we comment on two aspects of African climate highlighted by this comparison: (1) the relationship between Sahel and Gulf of Guinea rainfall, or between the African monsoon and the Atlantic ITCZ (also see Lebel et al. 2003; Biasutti et al. 2004; Gu and Adler 2004); (2) the role of the Indian Ocean in African climate variability (also see Bader and Latif 2003; Hoerling et al. 2004). Principal Component Analysis (PCA, in Section 3) applied to observations and to model output identified two distinct patterns of rainfall variability over tropical Africa during boreal summer. These patterns jointly explain about 40% of observed and 50% of the model's ensemble-mean variability. One represents variability at the northern edge of the seasonal monsoonal precipitation, in the semi-arid Sahel, between 10°N and 20°N. The other describes variability at the southern edge, along the Gulf of Guinea coast, between 10°N and the equator (see Fig. 2). Further analysis carried out on the ensemble of simulations indicates that they are also dynamically distinct. The Gulf of Guinea pattern owes its existence to tropical Atlantic Ocean variability only, more specifically to variability in eastern equatorial Atlantic SSTs, and is inextricably tied to the Atlantic marine ITCZ. The Sahel pattern represents variability in the African monsoon (Biasutti et al. 2004), and displays a non-negligible amount of noise, possibly intrinsic to chaotic land–atmosphere interaction. At the same time it is very sensitive to global, tropical oceanic conditions (Giannini et al. 2003). Consequently, the following remarks appear justified: (1) the Atlantic marine ITCZ is decoupled from the African monsoon; (2) variability in the Sahel represents variability in the accumulated total seasonal monsoon rains, as previously argued by Shinoda and Kawamura (1994), and not in the meridional migration of the location of convergence.

Long-term variability in Sahel rainfall is statistically related to variability in the oceans around Africa, especially the Indian Ocean. To connect changes in the Indian Ocean to the continental climate of the Sahel we find value in arguments about the contrast in thermodynamic properties between land and ocean (Chou et al. 2001), as well as in the classical description of the zonally symmetric, or Hadley circulation (Schneider 1977; Held and Hou 1980; Lindzen and Hou 1988; Plumb and Hou 1992), and in concepts related to equatorial wave dynamics (Matsuno 1966; Webster 1972; Gill 1980) applied to the zonally asymmetric circulation (Section 5).

Rainfall in the Sahel may have declined over the last 50 years as convection migrated from land to ocean, or as the zonal mean Hadley circulation migrated equatorward, attracted by a warming of the tropical oceans most conspicuous in the equatorial Indian Ocean. The questions that remain to be answered relate to the dynamical response of the atmosphere, and of the Asian–African monsoon in particular, to climate change. Since in the simulations considered here the direct radiative effect of anthropogenic greenhouse gases is not taken into account, it will be important to inter-

pret/anticipate how the monsoon will be affected by the transient and equilibrium responses of a rapidly responding land surface and slowly responding oceanic surface (Hansen et al. 2005). Will a warming of the tropical oceans successfully shift convection from land to ocean? Or will the Tibetan plateau warm enough, as perennial snow melts, to drive a stronger hemispheric monsoon?

Acknowledgments The authors wish to thank Max Suarez and Phil Pegion (NASA/GSFC) for their selfless scientific and technical support, and the two reviewers, Michela Biasutti and Guojun Gu, for their helpful, constructive comments. This study was supported by NASA's Seasonal to Interannual Prediction Project, through Interagency Agreement W-19,750 and by NOAA, through Grant NA16GP1575. PC was also supported by NOAA and NSF through research grants NA16GP1572, NA16GP2020, and ATM-0337846, and by the National Natural Science Foundation of China (NSFC) through Grant 40128003. The International Research Institute for climate prediction, a unit of the Earth Institute at Columbia University, is funded by a cooperative agreement between NOAA and Columbia University. The National Center for Atmospheric Research is operated by the University Corporation for Atmospheric Research under sponsorship of the National Science Foundation.

References

Bacmeister JT, Pegion PJ, Schubert SD, Suarez MJ (2001) Atlas of seasonal means simulated by the NSIPP1 atmospheric GCM. NASA Tech Memo 2000-104606 18, 100 pp

Bader J, Latif M (2003) The impact of decadal-scale Indian Ocean sea surface temperature anomalies on Sahelian rainfall and the North Atlantic Oscillation. Geophys Res Lett 30(22):2169 (doi: 10.1029/2003GL018426)

Barnett TP (2005) AAAS Annual Meeting, Washington, DC, 17 February 2005

Barnston AG, Mason SJ, Goddard L, DeWitt DG, Zebiak SE (2003) Multimodel ensembling in seasonal climate forecasting at IRI. Bull Am Meteorol Soc 84:1783–1796

Biasutti M, Battisti DS, Sarachik ES (2004) Mechanisms controlling the annual cycle of precipitation in the tropical Atlantic sector in an atmospheric GCM. J. Clim 17:4708–4723

Charney JG (1975) Dynamics of deserts and drought in the Sahel. Q J Roy Meteorol Soc 101:193–202

Chiang JCH, Sobel AH (2002) Tropical tropospheric temperature variations caused by ENSO and their influence on the remote tropical climate. J Clim 15:2616–2631

Chou C, Neelin JD (2004) Mechanisms of global warming impacts on regional tropical precipitation. J Clim 17:2688–2701

Chou C, Neelin JD, Su H (2001) Ocean–atmosphere–land feedbacks in an idealized monsoon. Q J Roy Meteorol Soc 127:1869–1891

Easterling DR, Peterson TC, Karl TR (1996) On the development and use of homogenized climate data sets. J Clim 9:1429–1434

Ellis WS, McCurry S (1987) Africa's Sahel, the stricken land. Natl Geogr 172:544–571

Englebert V (1974) Drought threatens the Touareg world. Natl Geogr April:140–179

Epstein ES (1969) A scoring system for probability forecasts of ranked categories. J Appl Meteorol 8:985–987

Folland CK, Palmer TN, Parker DE (1986) Sahel rainfall and worldwide sea temperatures. Nature 320:602–607

Folland CK, Shukla J, Kinter J, Rodwell M (2002) The Climate of the Twentieth Century Project. Clivar Exchanges 7:37–39

Fontaine B, Trzaska S, Janicot S (1998) Evolution of the relationship between near global and Atlantic SST modes and the rainy season in West Africa: statistical analyses and sensitivity experiments. Clim Dynam 14:353–368

Gadgil S, Joseph PV, Joshi NV (1984) Ocean–atmosphere coupling over monsoon regions. Nature 312:141–143

Gadgil S, Vinayachandran PN, Francis PA (2003) Droughts of the Indian summer monsoon: role of clouds over the Indian Ocean. Curr Sci 85:1713–1719

Gadgil S, Vinayachandran PN, Francis PA, Gadgil S (2004) Extremes of the Indian summer monsoon rainfall, ENSO and equatorial Indian Ocean Oscillation. Geophys Res Lett 31:L12213 (doi: 10.1029/2004GL019733)

Gates WL, Boyle J, Covey C, Dease C, Doutriaux C, Drach R, Fiorino M, Glecker P, Hnilo J, Marlais S, Phillips T, Potter G, Santer B, Sperber K, Taylor K, Williams D (1998) An overview of the results of the Atmospheric Model Intercomparison Project (AMIP I). Bull Am Meteorol Soc 73:1962:1970

Gerster G (1975) River of sorrow, river of hope. Natl Geogr August:152–189

Giannini A, Saravanan R, Chang P (2003) Oceanic forcing of Sahel rainfall on interannual to interdecadal time scales. Science 302:1027–1030 (doi: 10.1126/science.1089357)

Gill AE (1980) Some simple solutions for heat-induced tropical circulation. Q J Roy Meteorol Soc 106:447–462

Glantz MH, Katz RW (1985) Drought as a constraint to development in sub-Saharan Africa. AMBIO 14:334–339

Goddard L, Mason SJ (2002) Sensitivity of seasonal climate forecasts to persisted SST anomalies. Clim Dynam 19:619–631

Goddard L, Barnston AG, Mason SJ (2003) Evaluation of the IRI's "Net Assessment" seasonal climate forecasts: 1997–2001. Bull Am Meteorol Soc 84:1761–1781

Gu G, Adler RF (2004) Seasonal evolution and variability associated with the West African monsoon system. J Clim 17:3364–3377 (doi: 10.1175/1520-0442)

Hansen J, Nazarenko L, Ruedy R, Sato M, Willis J, DelGenio A, Koch D, Lacis A, Lo K, Menon S, Novakov T, Perlwitz Ju, Russell G, Schmidt G, Tausnev N (2005) Earth's energy imbalance: confirmation and implications. Science 308:1431–1435 (doi: 10.1126/science.1110252)

Hastenrath S, Lamb PJ (1977) Some aspects of circulation and climate over the eastern equatorial Atlantic. Mon Weather Rev 105:1019–1023

Held IM, Hou AY (1980) Nonlinear axially symmetric circulations in a nearly inviscid atmosphere. J Atmos Sci 37:515–533

Hoerling MP, Hurrell JW, Xu T, Bates GT, Phillips AS (2004) Twentieth century North Atlantic climate change. Part II: understanding the effect of the Indian Ocean warming. Clim Dynam 23:391–405

Houghton JT, Ding Y, Griggs DJ, Noguer M, van der Linden PJ, Dai X, Maskell K, Johnson CA (2001) Climate change 2001: the scientific basis. Cambridge University Press, Cambridge, p 811

Hurrell JW, Hoerling MP, Phillips AS, Xu T (2004) Twentieth century North Atlantic climate change. Part I: assessing determinism. Clim Dynam 23:371–389

Janicot S (1992) Spatiotemporal variability of West African rainfall. Part I: regionalizations and typings. J Clim 5:489–497

Janicot S, Moron V, Fontaine B (1996) Sahel droughts and ENSO dynamics. Geophys Res Lett 23:515–518

Janicot S, Trzaska S, Poccard I (2001) Summer Sahel–ENSO teleconnection and decadal time scale SST variations. Clim Dynam 18:303–320

Kirtman BP, Shukla J (2002) Interactive coupled ensemble: a new coupling strategy for CGCMs. Geophys Res Lett 29(10) (doi: 10.1029/2002GL014834)

Koster RD, Suarez MJ (1992) Modeling the land surface boundary in climate models as as composite of independent vegetation stands. J Geophys Res 97:2697–2715

Koster RD, Suarez MJ, Heiser M (2000) Variance and predictability of precipitation at seasonal-to-interannual timescales. J Hydrometeorology 1:26–46

Krishna Kumar K, Hoerling MP, Rajagopalan B (2005) Advancing dynamical prediction of Indian monsoon rainfall. Geophys Res Lett 32:L08704 (doi: 10.1029/2004GL021979)

Lamb PJ (1978a) Case studies of tropical Atlantic surface circulation patterns during recent sub-Saharan weather anomalies: 1967 and 1968. Mon Weather Rev 106:482–491

Lamb PJ (1978b) Large-scale tropical Atlantic surface circulation patterns associated with sub-Saharan weather anomalies. Tellus 30:240–251

Lebel T, Diedhiou A, Laurent H (2003) Seasonal cycle and interannual variability of the Sahelian rainfall at hydrological scales. J Geophys Res 108(8):8389 (doi: 10.1029/2001JD001580)

Lenters JD, Cook KH (1995) Simulation and diagnosis of the regional summertime precipitation climatology of South America. J Clim 8:2988–3005

Levitus S, Antonov JI, Boyer TP, Stephens C (2000) Warming of the world ocean. Science 287:2225–2229

Lindzen RS, Hou AY (1988) Hadley circulation for zonally averaged heating centered off the Equator. J Atmos Sci 45:2416–2427

Lough JM (1986) Tropical Atlantic sea surface temperatures and rainfall variations in sub-Saharan Africa. Mon Weather Rev 114:561–570

Matsuno T (1966) Quasi-geostrophic motions in the equatorial area. J. Meteorol Soc Jpn 44:25–43

Moorthi S, Suarez MJ (1992) Relaxed Arakawa–Schubert: a parameterization of moist convection for general circulation models. Mon Weather Rev 120:978–1002

Neelin JD, Chou C, Su H (2003) Tropical drought regions in global warming and El Niño teleconnections. Geophys Res Lett 30(24):2275 (doi: 10.1029/2003GL0018625)

Newell RE, Kidson JW (1984) African mean wind changes between Sahelian wet and dry periods. J Climatol 4:27–33

Nicholson SE (1979) Revised rainfall series for the West African subtropics. Mon Weather Rev 107:620–623

Nicholson SE (1980) The nature of rainfall fluctuations in West Africa. Mon Weather Rev 108:473–487

Nicholson SE (1993) An overview of African rainfall fluctuations of the last decade. J Clim 6:1463–1466

Nicholson SE, Grist JP (2001) A conceptual model for understanding rainfall variability in the West African Sahel on interannual and interdecadal timescales. Int J Climatol 21:1733–1757

Nicholson SE, Palao IM (1993) A re-evaluation of rainfall variability in the Sahel. Part I: characteristics of rainfall fluctuations. Int J Climatol 13:371–389

North GR, Bell TL, Callahan RF, Moeng FJ (1982) Sampling errors in the estimation of empirical orthogonal functions. Mon Weather Rev 110:699–706

Otterman J (1974) Baring high-albedo soils by overgrazing: a hypothesized desertification mechanism. Science 186:531–533

Palmer TN (1986) Influence of the Atlantic, Pacific and Indian Oceans on Sahel rainfall. Nature 322:251–253

Palmer TN and Co-authors (2004) Development of a European multimodel ensemble system for seasonal-to-interannual prediction (DEMETER). Bull Am Meteorol Soc 85:853–872

Peixoto JP, Oort AH (1992) Physics of climate. American Institute of Physics, New York

Peterson TC, Easterling DR (1994) Creation of homogeneous composite climatological reference series. Int J Climatol 14:671–679

Plumb RA, Hou AY (1992) The response of a zonally symmetric atmosphere to subtropical thermal forcing: threshold behavior. J Atmos Sci 49:1790–1799

Preisendorfer RW (1988). In: Mobley C (ed) Principal component analysis in meteorology and oceanography. Elsevier, Amsterdam, p 418

Rajagopalan B, Lall U, Zebiak SE (2002) Categorical climate forecasts through regularization and optimal combination of multiple GCM ensembles. Mon Weather Rev 130:1792–1811

Rao KG, Goswami BN (1988) Interannual variations of sea surface temperature over the Arabian Sea and the Indian summer monsoon: a new perspective. Mon Weather Rev 116:558–568

Rayner NA, Horton EB, Parker DE, Folland CK, Hackett RB (1996) Version 2.2 of the Global sea-Ice and Sea Surface Temperature Data Set: 1903–1994. Climate Research Technical Note. Unpublished document available from the Hadley Centre, UK

Rayner NA, Parker DE, Horton EB, Folland CK, Alexander LV, Rowell DP, Kent EC, Kaplan A (2003) Global analyses of sea surface temperature, sea ice, and night marine air temperature since the late nineteenth century. J Geophys Res 108(D14):4407

Reynolds RW, Smith TM (1994) Improved global sea surface temperature analyses using optimum interpolation. J Clim 7:929–948

Robertson AW, Lall U, Zebiak SE, Goddard L (2005) Improved combination of multiple atmospheric GCM ensembles for seasonal prediction. Mon Weather Rev 132:2723–2744

Rotstayn L, Lohmann U (2002) Tropical rainfall trends and the indirect aerosol effect. J Clim 15:2103–2116

Rowell DP (1998) Assessing potential seasonal predictability with an ensemble of multidecadal GCM simulations. J Clim 11:109–120

Rowell DP (2001) Teleconnections between the tropical Pacific and the Sahel. Q J Roy Meteorol Soc 127:1683–1706

Rowell DP, Folland CK, Maskell K, Ward MN (1995) Variability of summer rainfall over tropical North Africa (1906–1992): observations and modeling. Q J Roy Meteorol Soc 121:669–704

Schneider EK (1977) Axially symmetric steady-state models of the basic state for instability and climate studies. Part II: nonlinear calculations. J Atmos Sci 34:280–298

Schubert SD, Suarez MJ, Pegion PJ, Koster RD, Bacmeister JT (2004) On the cause of the 1930s Dust Bowl. Science 303:1855–1859

Shinoda M, Kawamura R (1994) Tropical rainbelt, circulation, and sea surface temperatures associated with the Sahelian rainfall trend. J Meteorol Soc Jpn 72:341–357

Su H, Neelin JD, Meyerson JE (2004) Mechanisms for lagged atmospheric response to ENSO SST forcing. Submitted to J Clim

Suarez MJ, Takacs LL (1995) Documentation of the ARIES/GEOS dynamical core: version 2. NASA Technical Memorandum 104606

Thomson MC, Palmer TN, Morse AP, Cresswell M, Connor SJ (2000): Forecasting disease risk with seasonal climate prediction. Lancet 355:1559–1560

Tippett MK, Giannini A (2005) Potentially predictable components of West African summer rainfall in a GCM simulation with observed SST. Submitted to J Clim

Traoré S (2003) A methodological note on crop yield forecasting in the Sahel. Paper presented at the Conference on Monsoon Environments: Agricultural and Hydrological Impacts of Seasonal Variability and Climate Change, International Centre for Theoretical Physics, Trieste, Italy, 24–28 March 2003

Vizy EK, Cook KH (2001) Mechanisms by which Gulf of Guinea and eastern North Atlantic Sea surface temperature anomalies can influence African rainfall. J Clim 14:795–821

Vizy EK, Cook KH (2002) Development and application of a mesoscale climate model for the tropics: influence of sea surface temperature anomalies on the West African monsoon. J Geophys Res 107(D3):4023 (doi: 10.1029/2001JD000686)

Von Storch H, Zwiers FW (1999) Statistical analysis in climate research. Cambridge University Press, Cambridge, p 484

Vose RS, Schmoyer RL, Steurer PM, Peterson TC, Heim R, Karl TR, Eischeid J (1992) The Global Historical Climatology Network: long-term monthly temperature, precipitation, sea level pressure, and station pressure data. ORNL/CDIAC-53, NDP-041. Carbon Dioxide Information Analysis Center, Oak Ridge National Laboratory, Oak Ridge, Tennessee, 300 pp

Wang G, Eltahir EAB, Foley JA, Pollard D, Levis S (2004) Decadal variability of rainfall in the Sahel: results from the coupled GENESIS–IBIS atmosphere biosphere system. Clim Dynam 22:625–637 (doi: 10.1007/s00382-004-0411-3)

Ward MN (1998) Diagnosis and short-lead time prediction of summer rainfall in tropical North Africa at interannual and multidecadal timescales. J Clim 11:3167–3191

Webster PJ (1972) Response of the tropical atmosphere to local, steady forcing. Mon Weather Rev 100:518–541

Webster PJ (2003) The coupled nature of intraseasonal and interannual monsoon variability. AMS Conference on Interactions of the Sea and Atmosphere

Wilks DS (1995) Statistical methods in the atmospheric sciences. Academic, New York, p 467

Wolter K (1989) Modes of tropical circulation, Southern Oscillation, and Sahel rainfall anomalies. J Clim 2:149–172

Xie P, Arkin PA (1997) Global precipitation: a 17-year monthly analysis based on gauge observations, satellite estimates and numerical model outputs. Bull Am Meteorol Soc 78:2539–2558

Yulaeva E, Wallace JM (1994) The signature of ENSO in global temperature and precipitation fields derived from the microwave sounding unit. J Clim 7:1719–1736

Zeng N, Neelin JD, Lau K-M, Tucker CJ (1999) Enhancement of interdecadal climate variability in the Sahel by vegetation interaction. Science 286:1537–1540

Zwiers FW (1996) Interannual variability and predictability in an ensemble of AMIP climate simulations conducted with the CCC GCM2. Clim Dynam 12:825–847